Analysis of High Gear Ratio Capabilities for Single-Stage, Series Multistage, and Compound Differential Coaxial Magnetic Gears

Matthew C. Gardner, *Student Member, IEEE*, Matthew Johnson, *Member, IEEE*, and Hamid A. Toliyat, *Fellow, IEEE*

***Abstract*--Magnetic gears perform the same fundamental power conversion as mechanical gears. However, magnetic gears have significant potential benefits due to their noncontact operation. This paper compares three different ways to achieve high gear ratios using coaxial magnetic gears by evaluating trends for radial flux coaxial magnetic gears with surface mounted permanent magnets. First, a single-stage design can be used, but the torque density and efficiency both decline as the gear ratio increases. Additionally, the gear ratio achievable with a single-stage coaxial magnetic gear is limited by practical considerations, such as the maximum number of modulators and pole pairs that can be used within the given space. Second, a multistage design can be formed by connecting single-stage designs in series. Multistage designs can achieve much higher net gear ratios with much less of a torque density penalty, especially as the number of stages increases, but this entails greater complexity. Third, the compound differential coaxial magnetic gear (CDCMG) is proposed. The CDCMG is formed by interconnecting two single-stage coaxial magnetic gears and can achieve gear ratios much higher than the product of the gear ratios of the individual stages. However, the circulating power in the CDCMG leads to poor efficiencies.**

***Index Terms*—Gear ratio, magnetic gear, multistage, optimization, torque density.**

I. Introduction

MAGNETIC gears convert mechanical power between high-torque, low-speed rotation and low-torque, high-speed rotation. However, whereas magnetic gears perform the same function as mechanical gears, magnetic gears rely on modulated magnetic fields, instead of direct contact, to transfer power. This noncontact operation gives magnetic gears a plethora of potential advantages over mechanical gears, including reduced maintenance, higher reliability, inherent overload protection, and physical isolation between shafts. Thus, significant research has focused on magnetic gears in recent years [1]-[4], and they have been proposed for a wide variety of high-torque, low-speed electromechanical energy conversion applications, such as wind energy [5], wave energy [6], [7], ship propulsion [8], and traction [9].

Most recent magnetic gear research focuses on coaxial magnetic gears [1]-[9]. Coaxial magnetic gears consist of three magnetically active cylindrical bodies, the low pole count rotor (Rotor 1), the modulators rotor (Rotor 2), and the high pole count rotor (Rotor 3), centered about the same axis, as illustrated in Fig. 1 for a radial flux, surface permanent magnet (PM) coaxial magnetic gear. To maximize the torque of the coaxial magnetic gear, the number of modulators (Q_2) is related to the number of pole pairs on the low pole count rotor (P_1) and on the high pole count rotor (P_3) by

$$Q_2 = P_1 + P_3. \tag{1}$$

If the design conforms to (1), the steady-state speeds of Rotor 1 (ω_1), Rotor 2 (ω_2), and Rotor 3 (ω_3) are governed by

$$P_1 \cdot \omega_1 - Q_2 \cdot \omega_2 + P_3 \cdot \omega_3 = 0. \tag{2}$$

Several different operating modes are possible, but fixing Rotor 3 results in the highest gear ratio, R, as given by

$$R = \frac{\omega_1}{\omega_2} = \frac{Q_2}{P_1}, \tag{3}$$

which relates the steady-state speeds of Rotor 1, the high speed rotor (ω_1), and Rotor 2, the low speed rotor (ω_2).

One of the primary advantages of using gears in high-torque, low-speed energy conversion applications is that it allows the electric machine to be much smaller than a direct-drive machine for the same application. The larger the gear

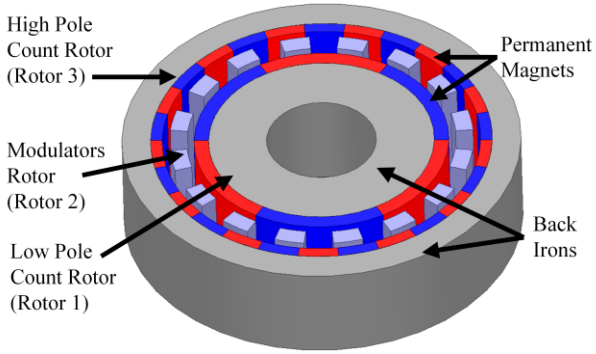

Fig. 1. Coaxial radial flux magnetic gear with surface mounted permanent magnets.

This work was supported in part by a Texas A&M Energy Institute Fellowship.

M. C. Gardner is with the Department of Electrical and Computer Engineering, Texas A&M University, College Station, TX 77843 USA (e-mail: gardner1100@tamu.edu).

M. Johnson was with the Department of Electrical and Computer Engineering, Texas A&M University, College Station, TX 77843 USA and is now with the Army Research Laboratory (e-mail: mjohnson11@tamu.edu).

H. A. Toliyat is with the Department of Electrical and Computer Engineering, Texas A&M University, College Station, TX 77843 USA (e-mail: toliyat@tamu.edu).

© IEEE 2018

ratio, the more the size of the electric machine can be reduced. However, most of the literature on coaxial magnetic gears focuses on designs with gear ratios less than 15:1, including several of the designs with the highest reported torque densities [1]-[10]. One alternative is to use cycloidal or harmonic magnetic gears, for which higher gear ratios have been demonstrated, but these topologies introduce additional mechanical challenges, such as unbalanced magnetic forces, eccentric rotation, or a mechanically deforming spline [11], [12]. This work uses 2D and 3D finite element analysis (FEA) to investigate three different means to achieve higher gear ratios using radial flux coaxial magnetic gears with surface mounted permanent magnets, such as the example shown in Fig. 1. First, single-stage magnetic gears with higher gear ratios are evaluated. Second, single-stage magnetic gears are connected in series to form multistage magnetic gears. Finally, two single-stage magnetic gears are interconnected to form the Compound Differential Coaxial Magnetic Gear (CDCMG). Although this study is limited to radial flux coaxial magnetic gears, many of the general trends analyzed in this work also apply to other coaxial flux magnetic gear variations (such as radial flux gears with flux focusing or Halbach array magnet configurations and axial and transverse flux coaxial magnetic gears of similar magnet configurations).

II. Single-Stage Coaxial Magnetic Gears

A multi-objective genetic algorithm was used to determine the Pareto optimal front maximizing both gear ratio and gravimetric torque density (GTD) in single-stage radial flux magnetic gears based on 2D FEA. Table I shows the range of values over which each design parameter was swept by the genetic algorithm, and Table II characterizes the materials used in the gears. The optimization was performed separately at each of the outer radii listed in Table III. As described in [13] and [14], G_R represents the integer part of the gear ratio and relates the pole pair counts according to

$$P_3 = \begin{cases} (G_R - 1) \cdot P_1 + 1 & \text{for } G_R \cdot P_1 \text{ odd} \\ (G_R - 1) \cdot P_1 + 2 & \text{for } G_R \cdot P_1 \text{ even} \end{cases}, \quad (4)$$

which eliminates unbalanced magnetic forces and keeps the cogging torque relatively low. Also, k_{PM} determines the ratio of the magnetic thicknesses on the low pole count rotor (T_{PM1}) and on the high pole count rotor (T_{PM3}) according to

$$T_{PM3} = k_{PM} \cdot T_{PM1}. \quad (5)$$

In general, a gear's stall torque is theoretically magnetically maximized by using the smallest possible air gap, but mechanical concerns, such as machining tolerances, limit the minimum air gap that can be achieved. Thus, as indicated in Table I, the air gaps are each fixed at 1 mm in this study as a compromise between these considerations. For other parameters, the ranges used in Table I are informed by the results presented in [13]. For example, the PM and modulator fill factors are not swept all the way from 0 to 1 but across smaller regions around the optimal values presented in [13].

Because end-effects can have a significant impact on the torque of coaxial magnetic gears [15], each of the optimal cross-sectional designs selected based on the 2D FEA simulation results was simulated at each of the stack lengths in Table III using 3D FEA. Then, for each of these optimal cross-sectional designs, the correct stack length necessary to achieve a low speed rotor stall torque of 1000 N·m was interpolated from the 3D FEA simulation results. For some of the smaller radii cases, the necessary stack length was beyond 100 mm and had to be extrapolated based on the torques at stack lengths of 80 mm and 100 mm. However, these stack lengths will still be fairly accurate since the torque becomes approximately linear at such high aspect ratios [15].

The GTD is calculated by dividing the low speed rotor stall torque by the total active mass, which is the sum of the masses of the back irons (made of M47 steel), the modulators (made of M47 steel), and the permanent magnets (made of N42 NdFeB). GTD is chosen for this study because, in addition to minimizing a design's active mass, optimizing for GTD tends to achieve a reasonable compromise between minimizing volume and minimizing active material cost [13]. As in [13] and [16], this study uses the GOSET genetic algorithm [17].

Fig. 2 shows the Pareto optimal front maximizing both gear ratio and GTD based on the design parameter value ranges provided in Table I at each of the outer radii in Table III. This Pareto optimal front indicates that, as the gear ratio increases, the maximum achievable gear GTD decreases. This presents the system designer with a fundamental tradeoff; as the gear ratio increases, the size of the electric machine decreases, but the size of the magnetic gear increases [7], [18]. The GTD of a system composed of a magnetic gear and an electric machine, GTD_{Sys}, is the magnetic gear's low speed rotor stall

TABLE I
Magnetic Gear Design Parameter Ranges

Name	Description	Range	Units
G_R	Integer part of gear ratio	3 – 31	
P_1	Rotor 1 pole pairs	3 – 25	
T_{BI1}	Rotor 1 back iron thickness	5 – 20	mm
T_{PM1}	Rotor 1 magnet thickness	3 – 12	mm
T_{AG}	Air gap thicknesses	1	mm
T_{Mods}	Modulator thickness	5 – 15	mm
k_{PM}	Magnet thickness ratio	0.5 – 1	
T_{BI3}	Rotor 3 back iron thickness	5 – 20	mm
α_{PM1}	Rotor 1 magnet tangential fill factor	0.75 – 1	
α_{Mods}	Modulators tangential fill factor	0.35 – 0.65	
α_{PM3}	Rotor 3 magnet tangential fill factor	0.75 – 1	

TABLE II
Magnetic Gear Active Material Characteristics

Material	Density	B_r
N42 NdFeB	7400 kg/m^3	1.3 T
M47 Steel (26 Gauge)	7870 kg/m^3	N/A

TABLE III
Magnetic Gear Design Discrete Parameter Values

Name	Description	Values	Units
r_{Out}	Magnetic gear outer radius	50, 75, 100, 150	mm
L_{Stack}	Stack length	5, 10, 15, 20, 25, 30, 40, 50, 60, 80, 100	mm

© IEEE 2018

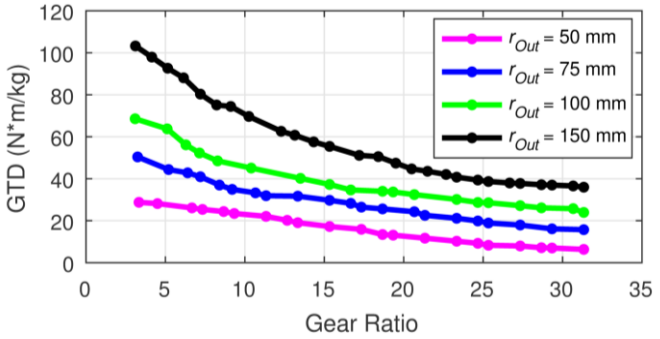

Fig. 2. Pareto optimal front maximizing the gear's GTD over a range of gear ratios and outer radii for a single-stage magnetic gear with a low speed rotor stall torque of 1000 N·m.

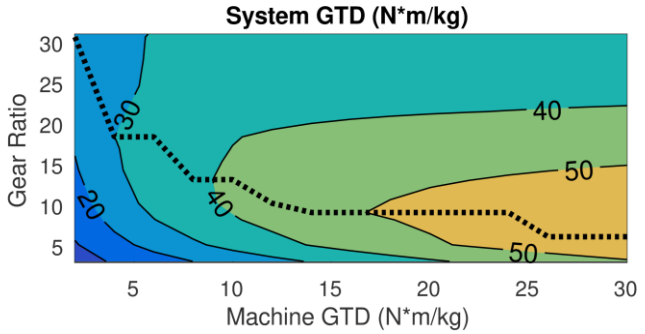

Fig. 3. Variation of the maximum achievable system GTD with gear ratio and machine GTD for systems with a low speed stall torque of 1000 N·m. The dashed line traces the maximum achievable system GTD and the corresponding gear ratio for each machine GTD.

torque, T_{Gear}, divided by the total active mass of the system, as given by

$$GTD_{Sys} = \frac{T_{Gear}}{M_{Gear} + M_{Machine}}, \tag{6}$$

where M_{Gear} and $M_{Machine}$ are the active masses of the magnetic gear and the electric machine, respectively. If the rated torque of the electric machine matches the stall torque of the gear's high speed rotor, which is T_{Gear}/R (where R is the gear ratio), GTD_{Sys} can be rewritten by expressing the masses of the magnetic gear and electric machine in terms of their respective GTDs, GTD_{Gear} and $GTD_{Machine}$, and factoring out T_{Gear} from both the numerator and denominator, which yields

$$GTD_{Sys} = \left(\left(GTD_{Gear} \right)^{-1} + \left(R \cdot GTD_{Machine} \right)^{-1} \right)^{-1}. \tag{7}$$

Fig. 3 illustrates the maximum system GTDs that can be achieved using the optimal 150 mm outer radius points in Fig. 2 and electric machines with different GTDs. The dashed line in Fig. 3 indicates the gear ratio that maximizes the system GTD for each machine GTD. Thus, a design with a relatively low gear ratio and a high torque density, such as those described in [1]-[10] may be less desirable from a system optimization standpoint than a gear with lower torque density, but a higher gear ratio. This is especially true for systems where the electric machine has a relatively low torque density. However, as the gear ratio increases, the number of modulators and stationary pole pairs increases; this increases manufacturing complexity and cost and may eventually result in components that are impractically thin in the tangential direction. Accordingly, the designer must evaluate several considerations in conjunction with the relevant electric machine scaling characteristics to select the appropriate design point which results in the optimal system configuration.

As the gear ratio changes, the optimal design parameters also change. The most significant change occurs in the number of Rotor 1 pole pairs, as shown in Fig. 4(a). Specifically, as the gear ratio increases, the optimal number of Rotor 1 pole pairs decreases to limit the increase in the number of Rotor 3 pole pairs and modulators because large numbers of Rotor 3 pole pairs or modulators result in excessive leakage flux. This reduction in the Rotor 1 pole count also reduces the flux leakage between adjacent magnets

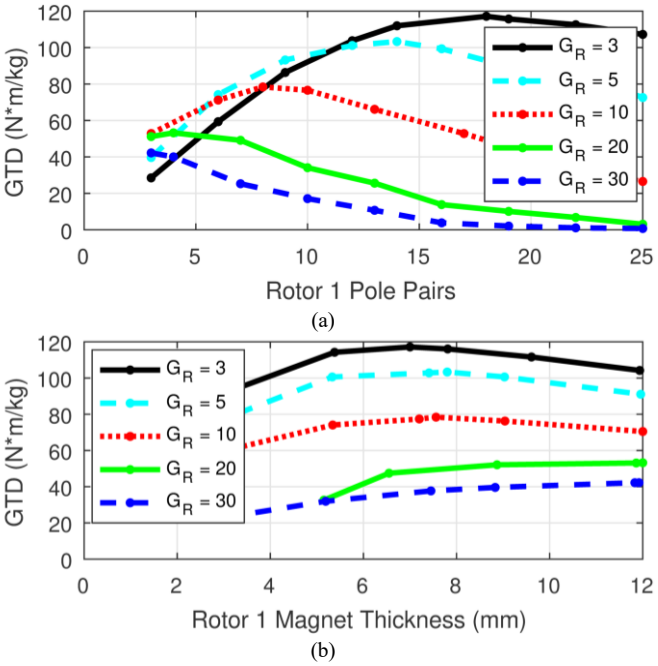

Fig. 4. Variation of the maximum achievable gear GTD at various G_R values with (a) the Rotor 1 pole pair count and (b) the Rotor 1 magnet thickness for designs with an outer radius of 150 mm based on 2D FEA.

on Rotor 1, which leads to an increase in the optimal Rotor 1 magnet thickness, as illustrated in Fig. 4(b).

Additionally, the gear ratio affects the gear's efficiency. Fig. 5 illustrates the variation of the full load electromagnetic efficiency with gear ratio and the low speed shaft speed for the 150 mm outer radius design points included in Fig. 2. Note that the electromagnetic efficiency calculations only account for the core losses (hysteresis and eddy current losses) in the back iron and modulator laminations and the eddy current losses in the magnets. These losses are calculated using 2D FEA and then scaled to the appropriate stack lengths based on the 3D FEA results. Efficiency decreases as speed increases because the eddy current losses increase with the square of the magnetic frequency, but the power rating only increases linearly with the speed. Additionally, efficiency decreases as the gear ratio increases, despite the fact that the optimal Rotor 1 pole count gradually decreases, which tends to lower the frequencies of the magnetic field harmonics. This efficiency reduction is partially due to the fact that for the same low

© IEEE 2018

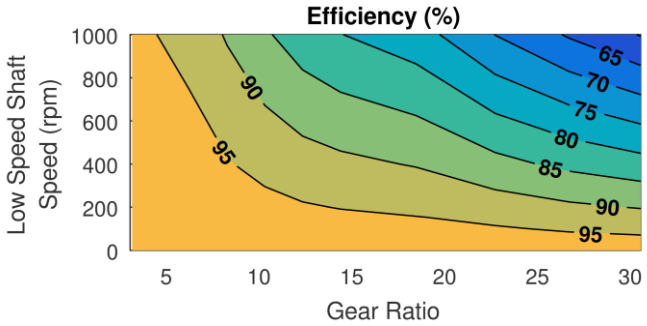

Fig. 5. Full load electromagnetic efficiencies of the optimal 150 mm outer radius points shown in Fig. 2 over a wide range of speeds.

speed shaft speed, a higher gear ratio yields a proportional increase in the high speed rotor speed, which results in a net increase in the magnetic frequencies. Furthermore, as illustrated by Fig. 2, higher gear ratio designs require more active material (both magnets and steel) to transmit the same torque, which results in higher losses.

III. Series Multistage Coaxial Magnetic Gears

Multiple single-stage coaxial magnetic gears can be connected in series to achieve a higher gear ratio than that which is practical with a single-stage coaxial magnetic gear [19]-[21]. If the high speed rotor of each stage is connected to the low speed rotor of the next stage, the net gear ratio is the product of the gear ratios of all the stages. Because each stage interacts with less torque than the previous stage (moving from the lowest speed rotor to the highest speed rotor), each subsequent stage can potentially be significantly smaller than the previous stage(s). (This study uses the convention that the low speed rotor of the first stage is connected to the low speed shaft of the multistage gearbox and the high speed rotor of the last stage is connected to the high speed shaft of the multistage gearbox.) Thus, as suggested in [19], successive stages could potentially be nested in the bore(s) of the preceding stage(s), which would result in a compact design. Although [19] only considers radial flux topologies, this idea could potentially be applied to other topologies, such as axial flux or transverse flux gears, or even with multiple different topologies used for different stages in the same gearbox.

The ratio between the torques needed for successive stages is ideally (assuming negligible losses) given by the gear ratio of the first (lowest speed) of the two stages; thus, the overall GTD of a multistage gear with n stages, GTD_{NET}, is given by

$$GTD_{NET} = \left((GTD_1)^{-1} + \sum_{i=2}^{n} \left(\left(GTD_i \cdot \prod_{j=1}^{i-1} R_j \right)^{-1} \right) \right)^{-1}, \quad (8)$$

where GTD_i is the GTD of the i^{th} stage and R_j is the gear ratio of the j^{th} stage, based on the convention that the first stage is the stage rated for the lowest speed and the highest torque, while the n^{th} stage is rated for the lowest torque and the highest speed. Based on (8), the cross-sectional designs along the Pareto optimal fronts in Fig. 2 can be connected in series to form the Pareto optimal fronts illustrated in Fig. 6 for multistage gearboxes with 2, 3, or 4 series-connected stages, which are shown in addition to the single-stage designs. As with the single-stage designs, the stall torque of the low speed shaft of each magnetic gearbox is 1000 N·m. The optimal design for each individual stage in each of these multistage gear designs was selected by interpolating between the 3D FEA results at the stack lengths in Table III to determine the correct stack length required for each of the optimal 2D cross-sectional designs to achieve the necessary torque for a given individual stage. For the later stages, which have lower torques, end-effects become more significant, especially at the larger outer radii. Thus, even though the largest outer radius designs are optimal for the first stage, as in Fig. 2, designs with smaller outer radii become optimal for the later stages with smaller torques, as shown in Fig. 6(a). This choice between smaller outer radii or more significant end-effects means that the later stages tend to have lower GTDs than the first stage; however, since these later stages are rated for lower torques, they contribute less to the overall mass of the gearbox and have a less significant effect on the overall gearbox GTD.

Fig. 6 shows that designs with more series-connected stages can achieve significantly higher net gear ratios and higher GTDs for a given net gear ratio, as compared to single-stage designs and multistage design with fewer stages. The colors of the points along the curves in Fig. 6(b) indicate the gear ratios used in the first (highest torque, lowest speed) stages of these optimal multistage gear designs. Because subsequent stages are rated for much smaller torques than the first stage, the mass of the first stage has the largest impact on the net GTD. Thus, it is advantageous to use a magnetic gear with a very high GTD for the first stage in order to minimize the total gearbox mass, even though that means that the first

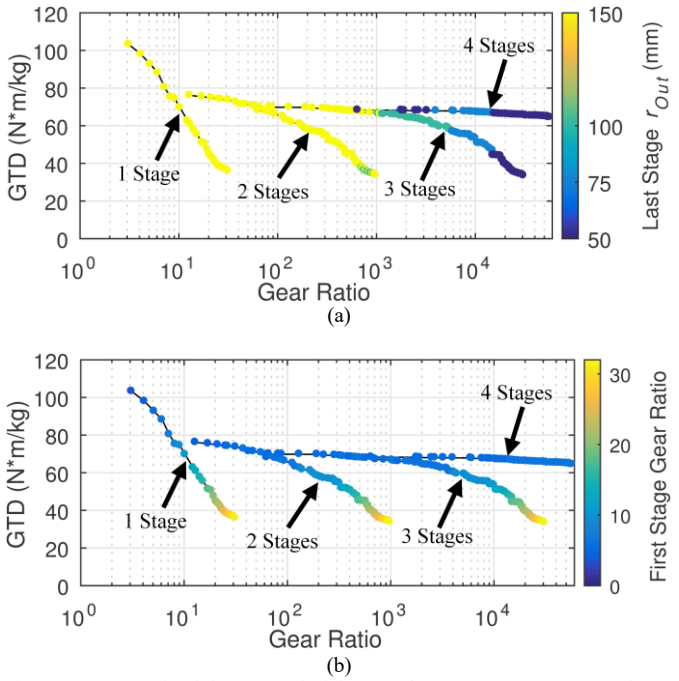

Fig. 6. Pareto optimal fronts maximizing gearbox GTD over a range of gear ratios for single-stage magnetic gearboxes and multistage magnetic gearboxes with 2, 3, or 4 series-connected stages and their (a) last stage outer radii and (b) first stage gear ratios.

© IEEE 2018

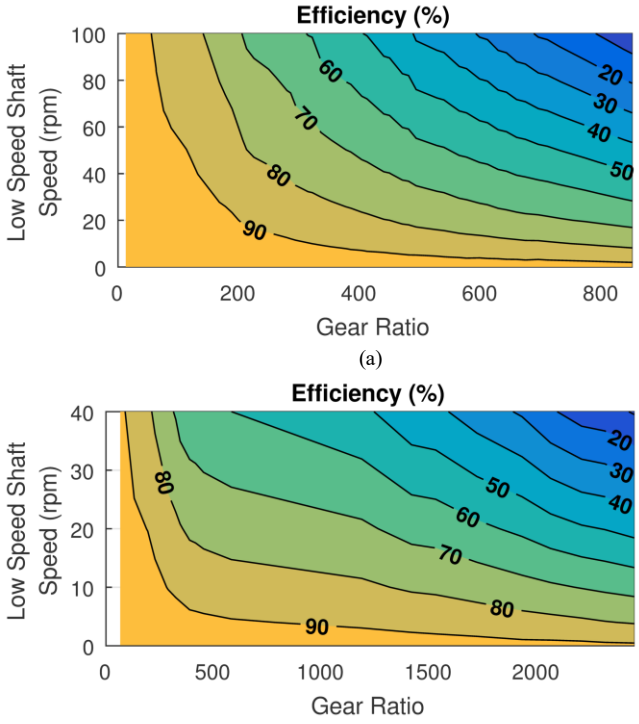

Fig. 7. Full load electromagnetic efficiencies of the optimal (a) 2-stage and (b) 3-stage coaxial magnetic gearboxes shown in Fig. 6.

stage has a relatively low gear ratio. Based on (8) and Fig. 6, it is apparent that the net gear ratio can theoretically be raised to a very large value with a minimal impact on net GTD by connecting a large number of high GTD, low gear ratio stages in series. However, this analysis neglects structural material and bearings. As the number of stages increases, more structural material and bearings are required, which increases the overall size, mass, and cost. Additionally, increasing the number of stages increases the gearbox complexity.

Fig. 7 illustrates the electromagnetic efficiencies of some of the maximum GTD 2-stage and 3-stage designs included in Fig. 6. Since the efficiency of each single-stage design has already been determined for a range of speeds, as shown in Fig. 5, the efficiency of each stage in the multistage design can be interpolated for its operating speed. The net efficiency of a series multistage design is simply the product of the efficiencies of each of its stages. Thus, as with the single-stage designs, the efficiencies of the multistage designs tend to decrease as the gear ratio or low speed shaft speed increases. Magnetically, the number of stages only has a small impact on the efficiency because the compounding effect of using more stages approximately cancels out the benefits of using lower gear ratio, higher efficiency designs for each stage.

IV. Compound Differential Coaxial Magnetic Gears

The single-stage coaxial magnetic gearbox can provide a high GTD at very low gear ratios, but the GTD decreases significantly as the gear ratio increases. Alternatively, a multistage magnetic gearbox can achieve much higher net gear ratios without as significant a reduction in GTD, especially with numerous stages; however, the multistage gearbox's complexity increases with the number of stages. The CDCMG provides an alternative that can combine two single-stage coaxial magnetic gears to achieve a net gear ratio much greater than the product of the individual stage gear ratios. Similarly to a compound mechanical planetary gear or the connection of two cycloidal magnetic gears proposed in [11], the CDCMG is formed by connecting two single-stage coaxial magnetic gears, as illustrated in the θ-z transverse-sections of a radial flux CDCMG in Fig. 8.

Although Fig. 8 only illustrates CDCMGs formed from radial flux coaxial gears, the CDCMG can be implemented with other coaxial topologies, such as axial or transverse flux gears, or even with a combination of two stages of different topologies. Additionally, there are multiple different ways to connect the two stages in a CDCMG, but the Free Spinning Rotor 3 (FSR3) configuration shown in Fig. 8(a) and the Free Spinning Rotor 2 (FSR2) configuration shown in Fig. 8(b) will generally provide the highest gear ratio. In the FSR3 configuration, the high speed shaft is connected to Rotor 1 in both stages, the Rotor 3s of the two stages are connected together and allowed to rotate freely, the Rotor 2 of Stage A is fixed in place, and the Rotor 2 of Stage B is connected to the

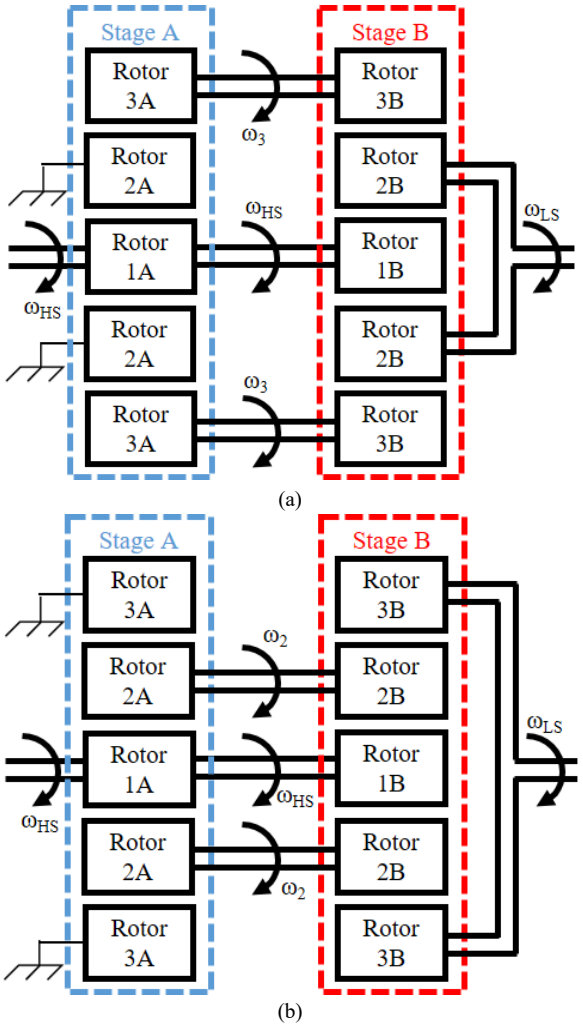

Fig. 8. θ-z transverse-sections of a radial flux CDCMG connected in the (a) Free Spinning Rotor 3 (FSR3) and (b) Free Spinning Rotor 2 (FSR2) configurations.

© IEEE 2018

low speed shaft. Similarly, in the FSR2 configuration, the high speed shaft is connected to Rotor 1 in both stages, the Rotor 2s of the two stages are connected together and allowed to rotate freely, the Rotor 3 of Stage A is fixed in place, and the Rotor 3 of Stage B is connected to the low speed shaft. For the FSR3 configuration, applying (2) to Stage A results in

$$\omega_3 = -\frac{P_{1A}}{P_{3A}} \cdot \omega_{HS}, \tag{9}$$

which relates the angular velocity of both Rotor 3s (ω_3) to the angular velocity of the high speed shaft (ω_{HS}). Applying (2) and (9) to Stage B yields

$$\omega_{LS} = \left(\frac{P_{1B}}{Q_{2B}} - \frac{P_{3B} \cdot P_{1A}}{Q_{2B} \cdot P_{3A}} \right) \cdot \omega_{HS}, \tag{10}$$

which relates the angular velocity of the low speed shaft (ω_{LS}) to that of the high speed shaft. Thus, the net gear ratio of the FSR3 configuration is given by

$$\text{FSR3 Gear Ratio} = \frac{\omega_{HS}}{\omega_{LS}} = \left(\frac{P_{1B}}{Q_{2B}} - \frac{P_{3B} \cdot P_{1A}}{Q_{2B} \cdot P_{3A}} \right)^{-1}. \tag{11}$$

Alternatively, the net gear ratio can be expressed as

$$\text{FSR3 Gear Ratio} = \frac{\omega_{HS}}{\omega_{LS}} = \frac{(R_A - 1) \cdot R_B}{R_A - R_B}, \tag{12}$$

where R_A and R_B are the gear ratios of Stage A and Stage B, as defined in (3). Thus, the net gear ratio of the CDCMG is essentially the product of the two single-stage gear ratios (R_A – 1 is the single-stage gear ratio of Stage A if the modulators are held stationary and Rotor 3 is allowed to rotate), divided by the difference between the two single-stage gear ratios.

A similar analysis for the FSR2 configuration yields

$$\text{FSR2 Gear Ratio} = \frac{\omega_{HS}}{\omega_{LS}} = \left(\frac{Q_{2B} \cdot P_{1A}}{Q_{2A} \cdot P_{3B}} - \frac{P_{1B}}{P_{3B}} \right)^{-1}. \tag{13}$$

The FSR2 configuration's gear ratio can also be expressed as

$$\text{FSR2 Gear Ratio} = \frac{\omega_{HS}}{\omega_{LS}} = \frac{(R_B - 1) \cdot R_A}{R_B - R_A}. \tag{14}$$

From (12) and (14), it is evident that the CDCMG's net gear ratio can be increased by increasing the gear ratios of the two stages and by decreasing the difference between the gear ratios of the two stages. However, increasing the gear ratio of each stage reduces the GTD of each stage. On the other hand, as shown in Fig. 4(a), lower gear ratios favor higher Rotor 1 pole counts, and, as indicated by (3), higher Rotor 1 pole counts allow for smaller increments of change in the gear ratio, which makes it possible to achieve smaller differences between the gear ratios of the two stages. Additionally, from (12) and (14), it is evident that the gear ratio of the FSR2 configuration is the same as that of the FSR3 configuration with Stages A and B interchanged; this means that both configurations can achieve the same gear ratios. However, the FSR3 configuration has an advantage with respect to GTD because the low speed shaft is connected to Rotor 2B, which has a higher stall torque than Rotor 3B. The ratio of the stall torques for these two configurations is $R_B/(R_B\text{-}1)$, which is especially significant if R_B is relatively small. Finally, (12) and (14) both indicate that if the gear ratios of the two stages are the same, then the CDCMG will ideally have an infinite gear ratio. In this case, the low speed shaft will have non-zero steady-state velocity only when slipping, and the high speed shaft will rotate freely, decoupled from the low speed shaft.

To illustrate the ability of the CDCMG to simultaneously achieve a high gear ratio and a relatively high GTD, an example radial flux CDCMG with a very aggressive gear ratio is presented, with the two stages connected in the FSR3 configuration. The parameters of Stages A and B are given as Design 1 in Table IV. Additionally, Design 2 is given as a design example with a less aggressive gear ratio. Both design examples are rated for a low speed stall torque of 1000 N·m. As in the previous sections, each design was optimized using 2D FEA; then, each design was evaluated at the stack lengths in Table III using 3D FEA, and the correct stack lengths were interpolated from the torques at the simulated stack lengths.

Design 1 combines two single-stage coaxial magnetic gears with gear ratios of 3.059 and 3.053 to achieve a net gear ratio of 1015 with a net GTD of 52.0 N·m/kg. For comparison, as indicated by the information in Figs. 2 and 6, a single-stage gear and a two stage series connected gear are generally incapable of practically achieving this high of a gear ratio with realistic magnet and modulator pole piece sizes and acceptable torque ripple characteristics. The largest gear ratio achieved by a two stage series connected gear considered in this study is 981.8 and that design only exhibits a GTD of 31.3 N·m/kg (with extremely high and relatively impractical single-stage gear ratios of 31.333 for both stages). Three and four stage series connected gears can achieve comparably high gear ratios over 1000, while maintaining high GTDs of 66.7

TABLE IV
CDCMG Design Examples

	Design 1		Design 2		
Name	**Stage A**	**Stage B**	**Stage A**	**Stage B**	**Units**
P_1	17	19	8	9	
Q_2	52	58	58	64	
P_3	35	39	50	55	
R	3.059	3.053	7.250	7.111	
r_{Out}	150	150	150	150	mm
T_{BI1}	5.0	5.0	6.9	6.0	mm
T_{PM1}	6.7	5.4	9.4	8.4	mm
T_{AG}	1	1	1	1	mm
T_{Mods}	5.0	5.0	5.2	5.0	mm
k_{PM}	0.80	0.78	0.51	0.52	
T_{BI3}	5.0	5.0	5.0	5.0	mm
α_{PM1}	0.86	0.94	0.79	0.75	
α_{Mods}	0.55	0.54	0.50	0.46	
α_{PM3}	0.92	0.95	0.93	0.84	
Stack Length	63.1	66.8	78.4	84.4	mm
GTD	103.4	104.3	75.6	78.5	N·m/kg
Net Gear Ratio	1015		320		
Net GTD	52.0		38.6		N·m/kg

© IEEE 2018

N·m/kg and 68.2 N·m/kg, respectively, but they require the added complexity associated with the additional gearing stages. Thus, the CDCMG is capable of achieving a very large net gear ratio with just two stages of relatively low gear ratios, while simultaneously maintaining a reasonable GTD. Alternatively, Design 2 combines two stages with gear ratios of 7.25 and 7.11 to achieve a much lower net gear ratio of 320 with a net GTD of 38.6 N·m/kg. This performance is quite achievable with a two stage series connected gear, but the CDCMG does have a slight advantage in the fact that each of its stages uses a lower gear ratio than what would be required in the stages of a series multistage solution.

However, the CDCMG suffers from poor efficiency. As shown in Fig. 9, at speeds above 1 rpm, Design 1 is less than 10% efficient and Design 2 is less than 50% efficient. This poor efficiency occurs because power circulates between the two stages, which means that each stage handles significantly more power than the amount transferred from the input shaft to the output shaft. Thus, even though the individual stages may have high efficiencies at their operating points, the net efficiency may be much lower than the product of the efficiencies of the two stages. The circulating power travels through the magnetic fields of Stage A, through the mechanical connection of the free spinning rotor between the two stages, through the magnetic fields of Stage B, and then through the mechanical connection of the high speed shaft between the stages. The power transferred between the stages through the free spinning rotor, P_{FSR}, is given by

$$P_{FSR} = \omega_{HS} \cdot \tau_{1A} , \tag{15}$$

where τ_{1A} is the torque on the high speed shaft from Stage A (assuming negligible electromagnetic losses in Stage A). In the FSR3 configuration, for there to be no steady-state net torque on the free spinning rotor, the torque on the high speed shaft from Stage B, τ_{1B}, must be given by

$$\tau_{1B} = -\frac{R_A - 1}{R_B - 1} \cdot \tau_{1A} , \tag{16}$$

assuming that the ratio of the torques between two rotors is given by the gear ratio between them. (This assumption is correct in the case of lossless transmission in each stage.) Thus, the net power on the high speed shaft, P_{HS}, is given by

$$P_{HS} = \omega_{HS} \cdot (\tau_{1A} + \tau_{1B}) = \left(1 - \frac{R_A - 1}{R_B - 1}\right) \cdot P_{FSR} . \tag{17}$$

If $R_A < R_B$, the circulating power, P_{circ}, is the difference between P_{FSR} and P_{HS} and is given by

$$P_{circ} = P_{FSR} - P_{HS} = \left(\frac{R_A - 1}{R_B - R_A}\right) \cdot P_{HS} . \tag{18}$$

However, if $R_A > R_B$, the circulating power is simply P_{FSR}, which is given by

$$P_{circ} = P_{FSR} = \left(\frac{R_B - 1}{R_B - R_A}\right) \cdot P_{HS} . \tag{19}$$

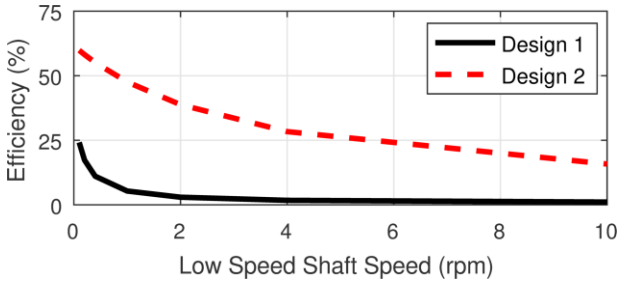

Fig. 9. Full load electromagnetic efficiencies for CDCMG Designs 1 and 2 in Table IV.

A similar analysis can be performed for the FSR2 configuration where $R_A - 1$ and $R_B - 1$ would be replaced with R_A and R_B, respectively. This analysis reveals a tradeoff involved in the selection of the gear ratios; as the difference between R_A and R_B decreases, the net gear ratio increases, but the efficiency also tends to decrease. As an example, Design 1 uses a smaller difference between R_A and R_B than Design 2 to achieve a higher net gear ratio, despite employing stages with smaller individual gear ratios, but Design 1 suffers from much higher losses. Additionally, if the difference between R_A and R_B is small, torque ripple may become a significant concern because the average net torque on the high speed shaft will be much smaller than the torques from each of the two stages.

The low efficiency caused by this circulating power makes the CDCMG impractical for most applications. However, at very low speeds, the efficiency is higher, so the CDCMG might be a reasonable solution for applications with very low speeds, such as a solar tracking system or a system to raise a drawbridge. Additionally, the CDCMG's use of lower single-stage gear ratios eliminates the need for an excessive number of modulators or Rotor 3 pole pairs. This provides more flexibility to pursue strategies to improve efficiency or reduce torque ripple, such as using a Halbach array on Rotor 3.

V. Conclusion

This paper evaluates three different options for achieving a high gear ratio using coaxial radial flux magnetic gears with surface permanent magnets. First, the gear ratio of a single-stage magnetic gear can be increased by increasing the ratio of the number of modulators to the number of pole pairs on the high speed rotor. However, as the gear ratio increases, both gravimetric torque density (GTD) and efficiency tend to decrease. Additionally, practical constraints limit the number of modulators and pole pairs that can be used, which limits the maximum gear ratio that can realistically be achieved. Second, multistage magnetic gearboxes can be formed by connecting single-stage designs in series. Connecting more gear stages in series allows a design to achieve very high gear ratios with a smaller reduction in GTD at the expense of increased complexity. To achieve a high GTD in a multistage gearbox, it is optimal to use a design with a relatively low gear ratio and a high GTD for the first stage connected directly to the low speed shaft. Because the other stages operate at much lower torques, they are much smaller and have less impact on the net GTD of the design. Third, the CDCMG can be formed by interconnecting two single-stage coaxial magnetic gears as

© IEEE 2018

shown in Fig. 8. This allows the CDCMG to achieve a much higher net gear ratio than the product of the gear ratios of the two stages. However, a significant amount of power circulates between these two stages, which results in a very low efficiency except at extremely low operating speeds.

This study provides an initial analysis of these three different means of achieving a high gear ratio. There are significant opportunities for further analysis in this area. This work only considers coaxial radial flux magnetic gears with surface permanent magnets. Although the trends presented in this paper will generally apply to other types of coaxial magnetic gears, future work could evaluate these trends more precisely for other types of coaxial magnetic gears. Furthermore, the fabrication and testing of prototype multistage magnetic gearboxes or CDCMGs would be a significant contribution. Finally, a CDCMG could be designed to achieve higher efficiency using techniques to reduce losses, such as using Halbach arrays.

VI. Acknowledgment

The authors would like to thank ANSYS for their generous support through the provision of FEA software.

VII. References

[1] K. Atallah and D. Howe, "A novel high-performance magnetic gear," *IEEE Trans. Magn.*, vol. 37, no. 4, pp. 2844–2846, Jul. 2001.

[2] N.W. Frank and H. A. Toliyat, "Analysis of the concentric planetary magnetic gear with strengthened stator and interior permanent magnet inner rotor," *IEEE Trans. Ind. Appl.*, vol. 47, no. 4, pp. 1652-1660, July/Aug. 2011.

[3] P. O. Rasmussen, T. O. Anderson, F. T. Jorgensen, and O. Nielsen, "Development of a High Performance Magnetic Gear," *IEEE Trans. Ind. Appl.*, vol. 41, no. 3, pp. 764-770, May/June 2005.

[4] P. M. Tlali, R.-J. Wang, and S. Gerber, "Magnetic gear technologies: A review," in *Proc. Int. Conf. Elect. Mach*., 2014, pp. 544–550.

[5] N. W. Frank and H. A. Toliyat, "Gearing ratios of a magnetic gear for wind turbines," in *Proc. IEEE Int. Elect. Mach. and Drives Conf.*, 2009, pp. 1224–1230.

[6] K. K. Uppalapati, J. Z. Bird, D. Jia, J. Garner, and A. Zhou, "Performance of a magnetic gear using ferrite magnets for low speed ocean power generation," in *Proc. IEEE Energy Convers. Congr. and Expo.*, 2012, pp. 3348–3355.

[7] M. Johnson, M. C. Gardner, H. A. Toliyat, S. Englebretson, W. Ouyang, and C. Tschida, "Design, Construction, and Analysis of a Large Scale Inner Stator Radial Flux Magnetically Geared Generator for Wave Energy Conversion," *IEEE Trans. Ind. Appl.*, vol. 54, no. 4, pp. 3305-3314, July/Aug. 2018.

[8] L. MacNeil, B. Claus, and R. Bachmayer, "Design and evaluation of a magnetically-geared underwater propulsion system for autonomous underwater and surface craft," in *Proc. Int. Conf. IEEE Oceans*, 2014, pp. 1-8.

[9] T. V. Frandsen, L. Mathe, N. I. Berg, R. K. Holm, T. N. Matzen, P. O. Rasmussen, and K. K. Jensen, "Motor integrated permanent magnet gear in a battery electrical vehicle," *IEEE Trans. Ind. Appl.*, vol. 51, no. 2, pp. 1516–1525, Mar./Apr. 2015.

[10] K. K. Uppalapati, M. D. Calvin, J. D. Wright, J. Pitchard, W. B Williams, and J. Z. Bird, "A Magnetic Gearbox With an Active Region Torque Density of 239 N·m/L," *IEEE Trans. Ind. Appl.*, vol. 54, no. 2, pp. 1331-1338, March/April 2018.

[11] J. Rens, K. Atallah, S. D. Calverley, and D. Howe, "A Novel Magnetic Harmonic Gear," *IEEE Trans. Ind. Appl.*, vol. 46, no. 1, pp. 206-212, Jan./Feb. 2010.

[12] F. T. Jorgensen, T. O. Andersen, and P. O. Rasmussen, "The Cycloid Permanent Magnetic Gear," *IEEE Trans. Ind. Appl.*, vol. 44, no. 6, pp. 1659-1665, Nov./Dec. 2008.

[13] M. C. Gardner, B. E. Jack, M. Johnson, and H. A. Toliyat, "Comparison of Surface Mounted Permanent Magnet Coaxial Radial Flux Magnetic Gears Independently Optimized for Volume, Cost, and Mass," *IEEE Trans. Ind. Appl.*, vol. 54, no. 3, pp. 2237-2245, May/June 2018.

[14] M. Johnson, M. C. Gardner, and H. A. Toliyat, "Design Comparison of NdFeB and Ferrite Radial Flux Surface Permanent Magnet Coaxial Magnetic Gears," *IEEE Trans. Ind. Appl.*, vol. 54, no. 2, pp. 1254-1263, March/April 2018.

[15] S. Gerber and R-J. Wang, "Analysis of the end-effects in magnetic gears and magnetically geared machines," in *Proc. IEEE Int. Conf. Elect. Mach.*, 2014, pp. 396-402.

[16] J. M. Crider, and S. D. Sudhoff, "An Inner Rotor Flux-Modulated Permanent Magnet Synchronous Machine for Low-Speed High-Torque Applications," *IEEE Trans. Energy Convers.*, vol. 30, no. 3, pp. 1247-1254, Sept. 2015.

[17] S. D. Sudhoff and Y. Lee, "Energy systems analysis consortium (ESAC) genetic optimization system engineering tool (GOSET) version manual," School Electr. Comput. Eng., Purdue Univ., West Lafayette, IN, 2003.

[18] M. Johnson, M. C. Gardner and H. A. Toliyat, "Design and Analysis of an Axial Flux Magnetically Geared Generator," *IEEE Trans. Ind. Appl.*, vol. 53, no. 1, pp. 97-105, Jan.-Feb. 2017.

[19] M. Filippini and P. Alotto, "Coaxial magnetic gears design and optimization," *IEEE Trans. Ind. Elect*., vol. 64, no. 12, pp. 9934-9942.

[20] M. Desvaux, B. Multon, H. B. Ahmed, S. Sire, A. Fasquelle, and D. Laloy, "Gear ratio optimization of a full magnetic indirect drive chain for wind turbine applications," in *Proc. Twelfth Int. Conf. Ecological Veh. Renewable Energies*, 2017, pp. 1-9.

[21] K. Li, J. Wright, S. Modaresahmadi, D. Som, W. Williams and J. Z. Bird, "Designing the first stage of a series connected multistage coaxial magnetic gearbox for a wind turbine demonstrator," in *Proc. IEEE Energy Convers. and Congr. Expo.*, 2017, pp. 1247-1254.

VIII. Biographies

Matthew C. Gardner (S'15) earned his B.S. in electrical engineering with a minor in computer science from Baylor University, Waco, Texas in 2014. He is currently pursuing a Ph.D. in electrical engineering while working in the Advanced Electric Machines and Power Electronics Laboratory at Texas A&M University. His research interests include optimal design and control of magnetic gears and magnetically geared machines.

Matthew Johnson (S'13, M'17) earned his B.S. in electrical engineering with a minor in mathematics from Texas A&M University, College Station, Texas in 2011. In 2017, he received a Ph.D. in electrical engineering while working in the Advanced Electric Machines and Power Electronics Laboratory at Texas A&M University. He is currently a research engineer at the Army Research Laboratory. His research interests include magnetic gears, magnetically geared machines, and motor drives.

Hamid A. Toliyat (S'87, M'91, SM'96, F'08) received the B.S, degree from Sharif University of Technology, Tehran, Iran in 1982, the M.S. degree from West Virginia University, Morgantown, WV in 1986, and the Ph.D. degree from University of Wisconsin-Madison, Madison, WI in 1991, all in electrical engineering. Following receipt of the Ph.D. degree, he joined the faculty of Ferdowsi University of Mashhad, Mashhad, Iran as an Assistant Professor of Electrical Engineering. In March 1994 he joined the Department of Electrical and Computer Engineering, Texas A&M University where he is currently the Raytheon endowed professor of electrical engineering. Dr. Toliyat has many papers and awards to his name, including the Nikola Tesla Field Award.

© IEEE 2018